PERGAMON

International Journal of Heat and Mass Transfer 42 (1999) 4299–4305

International Journal of HEAT and MASS TRANSFER

www.elsevier.com/locate/ijhmt

Effect of radiation on natural convection about a truncated cone

K.A. Yih

Department of General Course, Air Force Aeronautics Technology School, Kangshan, Kaohsiung, Taiwan 90395-2, ROC

Received 29 October 1998; received in revised form 9 March 1999

Abstract

A boundary layer analysis is presented to investigate numerically the effect of radiation on natural convection flow of an optically dense viscous fluid over an isothermal truncated cone in this paper. The nonsimilar governing equations are obtained by using a suitable transformation and solved by the Keller box method. Numerical results for the dimensionless velocity profiles, the dimensionless temperature profiles, the local friction coefficient and the local Nusselt number are graphically presented for the dimensionless distance ξ, the Prandtl number $Pr = 0.7$, the radiation–conduction parameter R_d and the surface temperature parameter H. It is shown that increasing ξ, R_d and H increases the local Nusselt number. The local friction coefficient decreases with increasing the above three parameters. Whereas, for the larger value of R_d and H, the variation of the local friction coefficient with ξ has the phenomenon of maximum. Furthermore, the local friction coefficient and the local Nusselt number of the truncated cone approach those of the inclined plate (full cone) for the case of $\xi = 0$ ($\xi \to \infty$).

1. Introduction

The problem of natural convection about heated vertical surfaces has received a great deal of attention. In the aspect of a vertical flat plate, Churchill and Ozoe [1] presented a correlation for laminar natural convection from a vertical plate. Kao [2] investigated the local nonsimilar solution for laminar natural convection adjacent to a vertical wall. The problem of natural convection over a semi-infinite flat plate with a non-uniform wall temperature is studied by Na [3] by a numerical method. Minkowycz and Sparrow [4] used the local nonsimilarity method to analyze laminar natural convection from a vertical plate.

In the aspect of a cone, Hering and Grosh [5] studied the laminar natural convection from a non-isothermal cone and showed that similarity solutions exist when the cone wall temperature varies as a power function of distance along a cone ray. Later, Hering [6] extended the analysis to investigate for low Prandtl numbers. Roy [7] extended the study of Hering and Grosh [5] to treat the case of high Prandtl numbers. Alamgir [8] used an integral method to study the overall heat transfer from vertical cones in laminar natural convection. Na and Chiou [9] investigated the laminar natural convection over a slender vertical frustum of a cone with a transverse curvature effect. Later, Na and Chiou [10] presented the laminar natural convection over a frustum of a cone without a transverse curvature effect (i.e., large cone angles when the boundary layer thickness is small compared with the local radius of the cone). They obtained the similarity solutions for the limiting cases of $\xi = 0$ and $\xi = \infty$, respectively. (ξ measures a dimensionless distance from the apex of the full cone.) Previous researches [1–10], however, have only concentrated upon the problem of natural convection without radiation effect.

As the difference between the surface temperature

0017-9310/99/$ - see front matter
PII: S0017-9310(99)00092-7

Nomenclature

a_r	Rosseland mean extinction coefficient
C_f	local friction coefficient, $2\nu(\partial u/\partial y)_{y=0}/U_r^2$
C_p	specific heat at constant pressure
f	dimensionless stream function
g	gravitational acceleration
Gr_{x^*}	local Grashof number, $g\cos\gamma\beta(T_w-T_\infty)(x^*)^3/\nu^2$
h	local heat transfer coefficient
H	surface temperature parameter, T_w/T_∞
k	thermal conductivity
Nu_{x^*}	local Nusselt number, hx^*/k
Pr	Prandtl number, ν/α
r	local radius of the truncated cone
R_d	radiation–conduction parameter, $4\sigma T_\infty^3/[k(a_r+\sigma_s)]$
T	temperature
u	velocity component in the x-direction
U_r	reference velocity, $[g\cos\gamma\beta(T_w-T_\infty)x^*]^{1/2}$
v	velocity component in the y-direction
x	streamwise coordinate
x_o	distance of the leading edge of truncated cone measured from the origin
x^*	distance measured from the leading edge of the truncated cone, $x-x_o$
y	transverse coordinate.

Greek symbols

α	thermal diffusivity
β	coefficient of thermal expansion
γ	half angle of the truncated cone
η	pseudosimilarity variable
θ	dimensionless temperature
ξ	dimensionless distance
ν	kinematic viscosity
ρ	density
σ	Stefan–Boltzmann constant
σ_s	scattering coefficient
ψ	stream function.

Subscripts

r	reference condition
w	condition at the wall
∞	condition at infinity.

and the ambient temperature is large, the radiation effect becomes important. In the aspect of convection–radiation, Viskanta and Grosh [11] considered the effects of thermal radiation on the temperature distribution and the heat transfer in an absorbing and emitting media flowing over a wedge by using the Rosseland diffusion approximation. This approximation leads to a considerable simplification in the expression for radiant flux. Later, a natural convection–radiation interaction in the boundary-layer flow over horizontal surfaces was presented by Ali et al. [12]. In [11,12], the temperature differences within the flow are assumed to be sufficiently small such that T^4 may be expressed as a linear function of temperature, i.e. $T^4 \simeq 4T_\infty^3 T - 3T_\infty^4$. Recently, Hossain and his fellow workers investigated the natural convection–radiation interaction on a boundary-layer flow along a thin vertical cylinder [13], an isothermal plate inclined at a small angle to the horizontal [14], and cylinders of an elliptic cross section [15], respectively. In [12–15], the implicit finite difference method together with the Keller box elimination technique was employed.

The purpose of this paper, therefore, is to extend the study of Na and Chiou [10] to consider the effect of radiation on the flow and heat transfer characteristics in a natural convection flow of an optically dense viscous fluid over an isothermal truncated cone.

2. Analysis

Consider the problem of the radiation effect on a natural convection boundary-layer flow of optically dense viscous incompressible fluid about a truncated cone (with half angle γ). Fig. 1 shows the flow model and physical coordinate system. The origin of the coor-

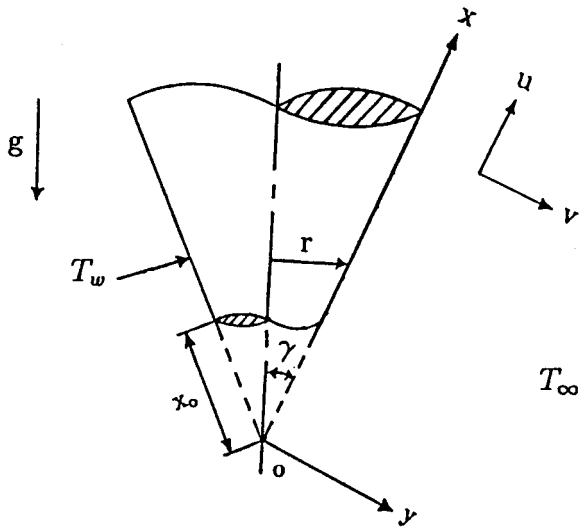

Fig. 1. The flow model and physical coordinate system.

dinate system is placed at the vertex of the full cone, where x is the coordinate along the surface of the cone measured from the origin and y is the coordinate normal to the surface, respectively. The boundary layer is assumed to develop at the leading edge of the truncated cone ($x=x_o$), which means the temperature at the circular base is assumed to be at the same as the ambient temperature T_∞. The uniform wall temperature of the truncated cone T_w is higher than T_∞, an upward flow is created as a result of the buoyancy force. The flow is laminar, steady and all the fluid properties are assumed to be constant except for the density variation in the buoyancy force term.

Introducing the boundary layer, Boussinesq and Rosseland diffusion approximations [13–15], the governing equations can be written as follows:

$$\frac{\partial(ru)}{\partial x}+\frac{\partial(rv)}{\partial y}=0, \tag{1}$$

$$u\frac{\partial u}{\partial x}+v\frac{\partial u}{\partial y}=g\cos\gamma\beta(T-T_\infty)+\nu\frac{\partial^2 u}{\partial y^2}, \tag{2}$$

$$u\frac{\partial T}{\partial x}+v\frac{\partial T}{\partial y}=\alpha\frac{\partial^2 T}{\partial y^2}+\frac{16\sigma}{3(a_r+\sigma_s)\rho C_p}\frac{\partial}{\partial y}\left(T^3\frac{\partial T}{\partial y}\right). \tag{3}$$

The boundary conditions are defined as follows:

$$y=0:\quad u=0,\quad v=0,\quad T=T_w, \tag{4}$$

$$y\to\infty:\quad u=0,\quad T=T_\infty, \tag{5}$$

where u and v are the velocities in the x- and y-directions. g is the gravitational acceleration. β is the thermal expansion coefficient. T is the temperature. ν is the kinematic viscosity. α is the thermal diffusivity. σ is the Stefan–Boltzmann constant. a_r is the Rosseland mean extinction coefficient. σ_s is the scattering coefficient. ρ is the density. C_p is the specific heat at constant pressure. The term $16\sigma T^3/[3(a_r+\sigma_s)]$ can be considered as the 'radiative conductivity'.

The boundary layer remains thin because it grows less quickly than does the radius of the cone. The local radius to a point in the boundary layer, therefore, can be replaced by the radius of the truncated cone r, i.e., $r=x\sin\gamma$. Eqs. (1)–(5) are valid in $x_o\le x<\infty$.

The continuity equation may be satisfied by introducing a stream function by the customary definition

$$ru=\frac{\partial\psi}{\partial y}\quad\text{and}\quad rv=-\frac{\partial\psi}{\partial x}. \tag{6}$$

Invoking the following dimensionless variables

$$\xi=\frac{x^*}{x_o}=\frac{x-x_o}{x_o},\quad \eta=\frac{y}{x^*}(Gr_{x^*})^{1/4},$$
$$f(\xi,\eta)=\frac{\psi}{\nu r(Gr_{x^*})^{1/4}},\quad \theta(\xi,\eta)=\frac{T-T_\infty}{T_w-T_\infty} \tag{7}$$

and substituting Eq. (7) into Eqs. (1)–(5), we obtain

$$f'''+\left(\frac{\xi}{1+\xi}+\frac{3}{4}\right)ff''-\frac{1}{2}(f')^2+\theta=\xi\left(f'\frac{\partial f'}{\partial\xi}-f''\frac{\partial f}{\partial\xi}\right), \tag{8}$$

$$\frac{1}{Pr}\theta''+\left(\frac{\xi}{1+\xi}+\frac{3}{4}\right)f\theta'+\frac{4R_d}{3\,Pr}\{\theta'[(H-1)\theta+1]^3\}'=\xi\left(f'\frac{\partial\theta}{\partial\xi}-\theta'\frac{\partial f}{\partial\xi}\right). \tag{9}$$

The boundary conditions are defined as follows:

$$\eta=0:\quad f'=0,\quad f=0,\quad \theta=1, \tag{10}$$

$$\eta\to\infty:\quad f'=0,\quad \theta=0. \tag{11}$$

Utilizing the transformation Eq. (7), the velocities in the x- and y-directions may be evaluated from Eq. (6) as

$$u=\frac{\nu(Gr_{x^*})^{1/2}}{x^*}f'=U_r f'\quad\text{and}$$

$$v=-\frac{\nu(Gr_{x^*})^{1/4}}{x^*}\left[\left(\frac{\xi}{1+\xi}+\frac{3}{4}\right)f+\xi\frac{\partial f}{\partial\xi}-\frac{1}{4}\eta f'\right]. \tag{12}$$

In the above equations, the primes denote the differentiation with respect to η. x^* is the distance measured from the leading edge of the truncated cone. $Gr_{x^*}=g\cos\gamma\beta(T_w-T_\infty)(x^*)^3/\nu^2$ is the local Grashof number based upon x^*. $Pr=\nu/\alpha$ is the Prandtl number. $R_d=4\sigma T_\infty^3/[k(a_r+\sigma_s)]$ is the radiation–conduction parameter. $H=T_w/T_\infty$ is the surface temperature parameter which represents the ratio of the surface temperature and the ambient temperature. $U_r=[g\cos\gamma\beta(T_w-T_\infty)x^*]^{1/2}$ is the reference velocity.

It is apparent that for the case of $R_d=0$ (no radiation interaction), Eqs. (8) and (9) are reduced to those of Na and Chiou [10]. For the case of $\xi=R_d=\gamma=0$, Eqs. (8) and (9) are reduce to those of a vertical plate [3] where the similarity solutions are obtained. For the case of $\xi\to\infty$, Eqs. (8) and (9)

reduce to the case of a full cone and the similarity solutions are also obtained since $\partial f/\partial\xi = \partial f'/\partial\xi = \partial\theta/\partial\xi = 0$ as $\xi \to \infty$.

3. Numerical method

Eqs. (8) and (9) with the boundary conditions (10) and (11) have been solved numerically using a very efficient implicit finite-difference method known as the modified Keller-box scheme [16]. The computations were carried out on an AcerPower 590hd computer. We have studied the effects of step sizes of $\Delta\xi$, $\Delta\eta_1$ and the edge of the boundary-layer η_∞ on the solution in order to optimize them. Therefore, the variable grid parameter is 1.01, $\Delta\eta_1 = 0.001$ and $\Delta\xi = 0.001$ $(0 \le \xi \le 0.01)$, 0.01 $(0.01 \le \xi \le 0.1)$, 0.1 $(0.1 \le \xi \le 1)$, 1 $(1 \le \xi \le 10)$, 10 $(10 \le \xi \le 100)$, 100 $(100 \le \xi \le 1000)$, 1000 $(1000 \le \xi \le 10{,}000)$. The edge of the boundary-layer $20 \le \eta_\infty \le 50$ is found to be sufficiently accurate for the values of $|f''_\infty|$, $|\theta'_\infty| < 10^{-3}$. The results here are independent of the step sizes of $\Delta\xi$, $\Delta\eta_1$ and η_∞ almost up to the fourth decimal place. The iterative procedure is stopped to give the velocity and the temperature distributions when the error in computing the $|f''_w|$ and $|\theta'_w|$ in the next procedure becomes less than 10^{-5}.

The integrated values of the velocity and the temperature fields from Eqs. (8) and (9) thus obtained are used to calculate the corresponding values of the local friction coefficient and the local Nusselt number from the following relations:

$$\frac{1}{2}C_f(Gr_{x^*})^{1/4} = -f''(\xi,0) \quad \text{and}$$
$$\frac{Nu_{x^*}}{(Gr_{x^*})^{1/4}} = \left(1 + \frac{4R_dH^3}{3}\right)[-\theta'(\xi,0)]. \tag{13}$$

4. Results and discussion

In order to verify the accuracy of our present method, we have compared our results with those of Cebeci and Bradshaw [17], Na [3], Na and Chiou [10], Kays and Crawford [18], Lin and Chen [19], Hering [6], Roy [7] and Alamgir [8]. The comparisons in all the above cases are found to be in excellent agreement, as shown in Table 1. Here, ∞ denotes $\xi = 10^4$.

Numerical results are presented graphically for the Prandtl number $Pr = 0.7$, the dimensionless distance ξ

Table 1
Comparison of values of (a) $f''(0, 0)$ and $-\theta'(0, 0)$ and (b) $f''(\infty, 0)$ and $-\theta'(\infty, 0)$ for various values of Pr with $R_d = 0$

(a)	$f''(0, 0)$		$-\theta'(0, 0)$					
Pr	[17]	Present results	[3]	[10]	[17]	[18]	[19]	Present results
0.0001	—	1.4998	—	—	—	—	—	0.0060
0.001	—	1.4728	—	—	—	—	0.0187	0.0189
0.01	—	1.3968	0.0574	0.0574	—	0.0570	0.0570	0.0570
0.1	1.2104	1.2144	—	—	0.1637	0.164	0.1627	0.1629
1	0.9081	0.9084	0.4010	0.4011	0.4009	0.401	0.4009	0.4012
10	0.5930	0.5927	0.8269	0.8269	0.8266	0.827	0.8258	0.8266
100	0.3564	0.3559	1.5493	1.5493	1.5495	1.55	1.5490	1.5493
1000	—	0.2049	—	—	—	2.80	2.8035	2.8035
10,000	—	0.1161	—	—	—	—	5.0125	5.0127

(b)	$f''(\infty, 0)$			$-\theta'(\infty, 0)$				
Pr	[6]	[7]	Present results	[6]	[7]	[8]	[10]	Present results
0.0001	—	—	1.6006	—	—	0.0071	—	0.0079
0.001	1.5166	—	1.5135	0.0247	—	0.0225	—	0.0246
0.01	1.3550	—	1.3551	0.0748	—	0.0709	0.0749	0.0749
0.1	1.0960	—	1.0960	0.2113	—	0.2141	—	0.2116
1	0.7694	0.8600	0.7699	0.5104	0.5275	0.5280	0.5104	0.5109
10	—	0.4899	0.4877	—	1.0354	1.0159	1.0340	1.0339
100	—	0.2897	0.2896	—	1.9229	1.8237	1.9220	1.9226
1000	—	0.1661	0.1661	—	3.4700	3.2463	—	3.4696
10,000	—	0.0940	0.0940	—	6.1998	5.7734	—	6.1984

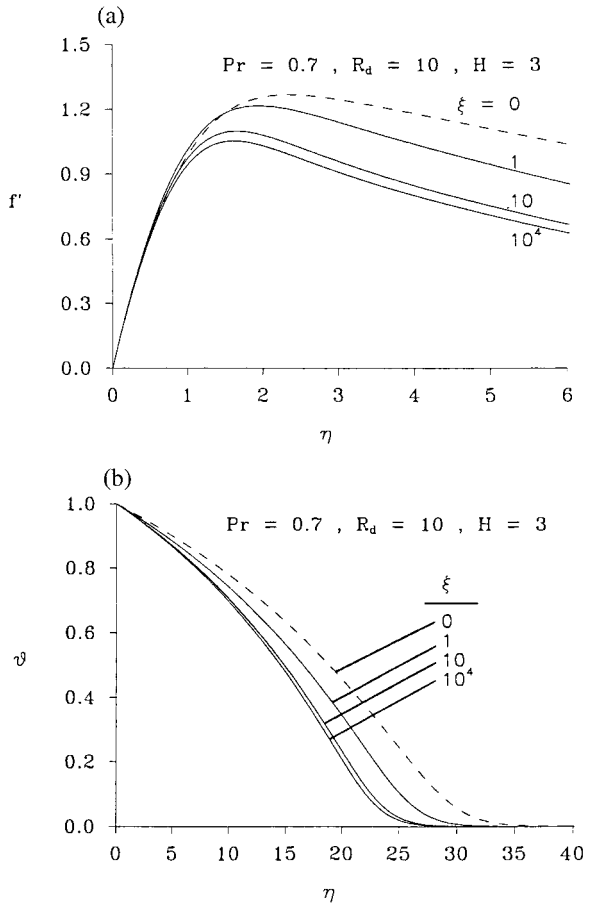

Fig. 2. Dimensionless (a) velocity and (b) temperature profiles for various values of R_d.

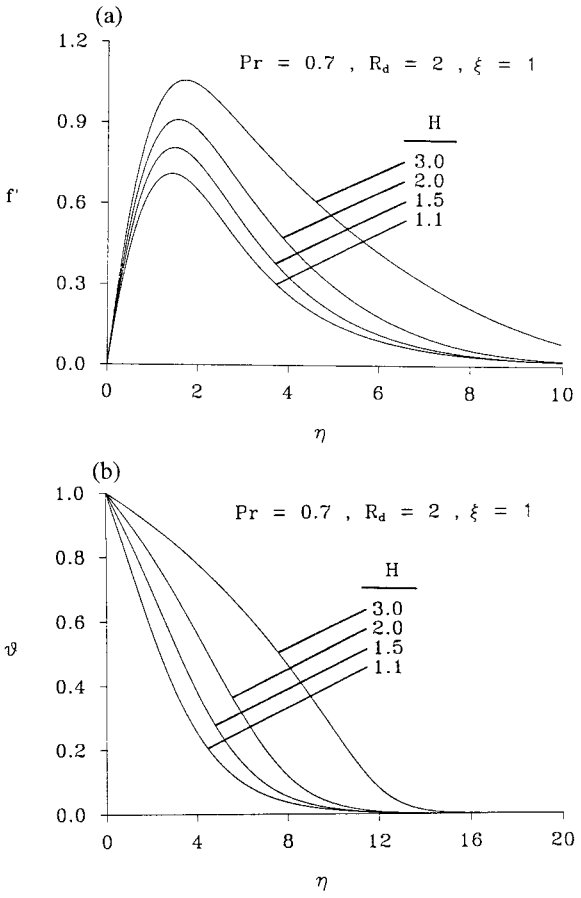

Fig. 3. Dimensionless (a) velocity and (b) temperature profiles for various values of H.

ranging from 10^{-3} to 10^4, the radiation–conduction parameter R_d ranging from 0 to 10 and the surface temperature parameter H ranging from 1.1 to 3.0.

Fig. 2 shows the dimensionless (a) velocity and (b) temperature profiles for various values of the radiation–conduction parameter R_d, respectively. The dimensionless velocity and temperature profiles become fat for the increase of R_d. Furthermore, both the maximum velocity and the location of the maximum velocity away from the surface increase as R_d increases.

The dimensionless (a) velocity and (b) temperature profiles for various values of the surface temperature parameter H are illustrated in Fig. 3, respectively. When H increases, the maximum velocity increases and the dimensionless velocity and temperature profiles become fat. When R_d and H are changed, the dimensionless velocity (temperature) profiles tend to be similar to Figs. 2(a) and 3(a) (Figs. 2(b) and 3(b)).

Fig. 4 depicts the dimensionless (a) velocity and (b) temperature profiles for various values of the dimensionless distance ξ, respectively. The dimensionless velocity and temperature profiles become thin for the increase of ξ. It is also found that, for the case of $\xi=1$, the dimensionless velocity gradient at the wall is larger than other cases, as presented in Fig. 4(a). Whereas, the dimensionless temperature gradient at the wall increases with increasing ξ.

The local (a) friction coefficient and (b) Nusselt number for various values of the radiation–conduction parameter R_d are shown in Fig. 5, respectively. For a fixed value of ξ, the local friction coefficient and the local Nusselt number increase as R_d increases. When ξ is very small and large, the local friction coefficient and the local Nusselt number become almost constant. For the case of $R_d=0.1$, the local friction coefficient reduces as ξ increases. While, for the case of $R_d=10$, as ξ varies from 10^{-3} to 10^4, the local friction coefficient increases initially from a constant value, reaches a maximum (about $\xi=2$) and then decreases gradually to another constant value. This is because the dimensionless wall velocity gradient at $\xi=1$ is larger, as

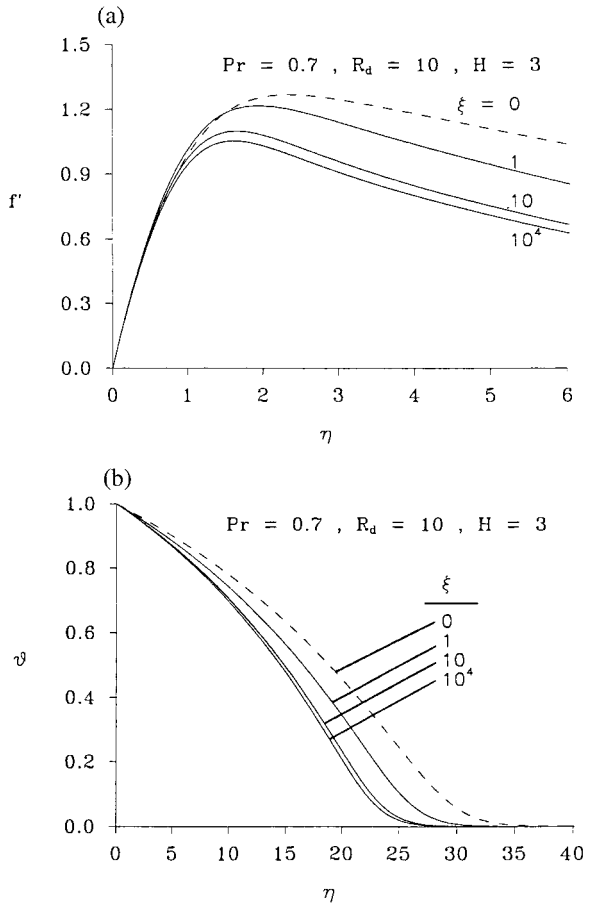

Fig. 4. Dimensionless (a) velocity and (b) temperature profiles for various values of ξ.

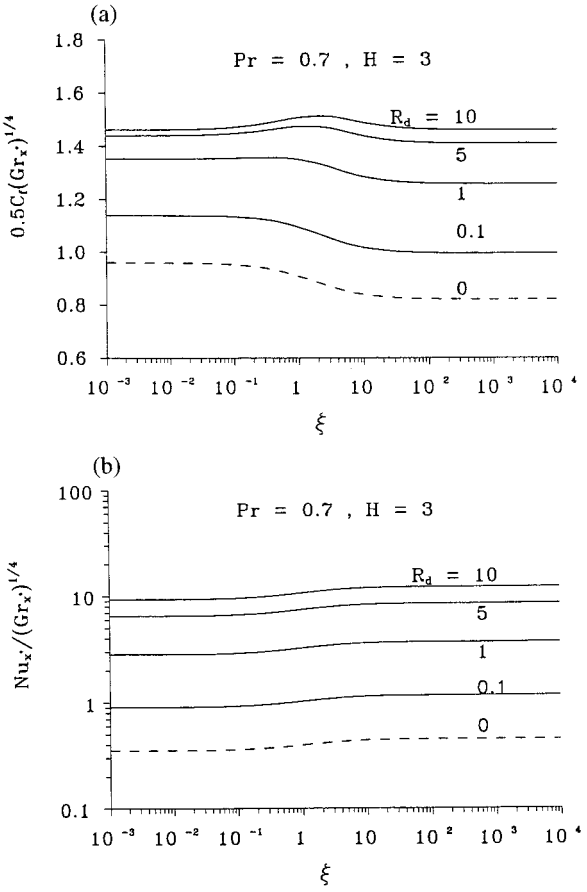

Fig. 5. Local (a) friction coefficient and (b) Nusselt number for various values of R_d.

revealed in Fig. 4(a). It is also apparent that, for a given R_d, the local Nusselt number enhances with increasing ξ, as shown in Fig. 5(b).

Fig. 6 displays the local (a) friction coefficient and (b) Nusselt number for various values of the surface temperature parameter H, respectively. For a fixed value of ξ, the local friction coefficient and the local Nusselt number increase as H increases. This is due to the fact that increasing R and H increases the surface velocity gradient $f''(\xi, 0)$, as shown in Figs. 2(a) and 3(a). The higher the surface velocity gradient is, the larger local friction coefficient. Although the surface temperature gradient $-\theta'(\xi, 0)$ is low for the case of large R_d and H (radiation effect becomes pronounced), as shown in Figs. 2(b) and 3(b), the local Nusselt number is still large. This is because the local Nusselt number is found to be significantly affected by R_d and H than $-\theta'(\xi, 0)$, as revealed in Eq. (13). For the case of $H = 3$, the variation of the local friction coefficient with ξ also has the phenomenon of maximum (about $\xi = 0.7$), as illustrated in Fig. 6(a). While, the local Nusselt number enhances from the lower constant to the higher one with the increase of ξ, as shown in Fig. 6(b).

5. Conclusions

The effect of radiation on the natural convection flow of an optically dense viscous fluid over an isothermal truncated cone with Rosseland diffusion approximation is numerically analyzed. The transformed governing equations are solved by the Keller box method. Numerical solutions for the details of the dimensionless velocity and temperature profiles, the local friction coefficient and the local Nusselt number are presented graphically for a range of the dimensionless distance ξ, the radiation–conduction parameter R_d and the surface temperature parameter H. For the larger value of R_d and H, as ξ varies from 10^{-3} to 10^4,

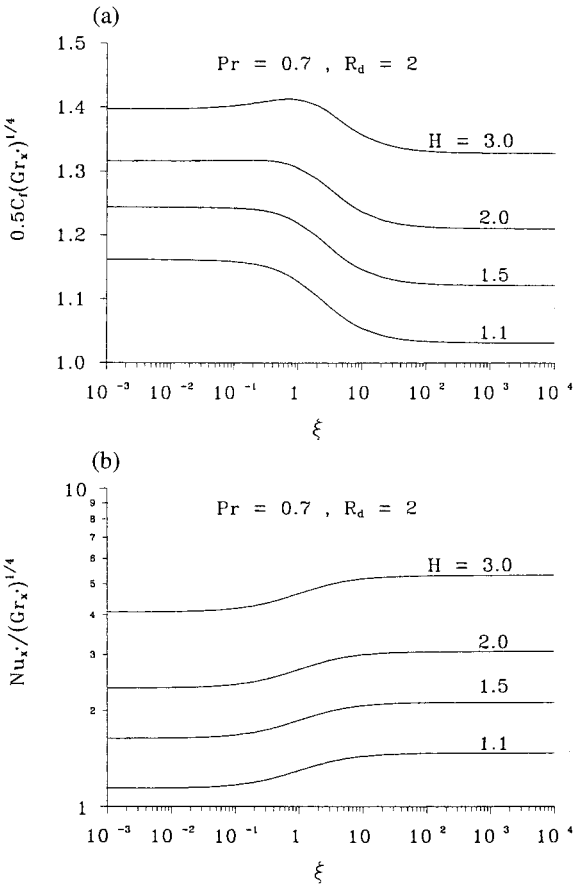

Fig. 6. Local (a) friction coefficient and (b) Nusselt number for various values of H.

the local friction coefficient increases initially from a higher constant value, reaches a maximum at an intermediate value of ξ and then decreases gradually to a lower constant value. Increasing the value of ξ, H and R_d augments the local Nusselt number. Moreover, the local friction coefficient and the local Nusselt number approach to the limits of the inclined plate (full cone) as ξ is very small (large).

References

[1] S.W. Churchill, H. Ozoe, A correlation for laminar free convection from a vertical plate, Transactions of ASME Journal of Heat Transfer 95 (1973) 540–541.

[2] T.T. Kao, Local nonsimilar solution for laminar free convection adjacent to a vertical wall, Transactions of ASME Journal of Heat Transfer 98 (1976) 321–322.

[3] T.Y. Na, Numerical solution of natural convection flow past a non-isothermal vertical flat plate, Applied Scientific Research 33 (1978) 519–543.

[4] W.J. Minkowycz, E.M. Sparrow, Numerical solution scheme for local nonsimilarity boundary layer analysis, Numerical Heat Transfer 1 (1978) 69–85.

[5] R.G. Hering, R.J. Grosh, Laminar free convection from a non-isothermal cone, International Journal of Heat and Mass Transfer 5 (1962) 1059–1068.

[6] R.G. Hering, Laminar free convection from a non-isothermal cone at low Prandtl numbers, International Journal of Heat and Mass Transfer 8 (1965) 1333–1337.

[7] S. Roy, Free convection from a vertical cone at high Prandtl numbers, Transactions of ASME Journal of Heat Transfer 96 (1974) 115–117.

[8] M. Alamgir, Over-all heat transfer from vertical cones in laminar free convection: an approximate method, Transactions of ASME Journal of Heat Transfer 101 (1979) 174–176.

[9] T.Y. Na, J.P. Chiou, Laminar natural convection over a slender vertical frustum of a cone, Wärme- und Stoffübertragung 12 (1979) 83–87.

[10] T.Y. Na, J.P. Chiou, Laminar natural convection over a frustum of a cone, Applied Scientific Research 35 (1979) 409–421.

[11] R. Viskanta, R.J. Grosh, Boundary layer in thermal radiation absorbing and emitting media, International Journal of Heat and Mass Transfer 5 (1962) 795–806.

[12] M.M. Ali, T.S. Chen, B.F. Armaly, Natural convection–radiation interaction in boundary-layer flow over horizontal surfaces, AIAA Journal 22 (1984) 1797–1803.

[13] M.A. Hossain, M.A. Alim, Natural convection–radiation interaction on boundary layer flow along a thin vertical cylinder, Heat and Mass Transfer 32 (1997) 515–520.

[14] M.A. Hossain, D.A.S. Rees, Free convection–radiation interaction from an isothermal plate inclined at a small angle to the horizontal, Acta Mechanica 127 (1998) 63–73.

[15] M.A. Hossain, M.A. Alim, D.A.S. Rees, Effect of thermal radiation on natural convection over cylinders of elliptic cross section, Acta Mechanica 129 (1998) 177–186.

[16] T. Cebeci, P. Bradshaw, Momentum Transfer in Boundary Layer, 1st ed., Hemisphere, Washington, 1977, p. 213.

[17] T. Cebeci, P. Bradshaw, Physical and Computational Aspects of Convective Heat Transfer, 1st ed. Springer, New York, 1984, p. 270.

[18] W.M. Kays, M.E. Crawford, Convective Heat and Mass Transfer, 3rd ed., McGraw-Hill, New York, 1980, p. 402.

[19] H.T. Lin, C.C. Chen, Mixed convection on vertical plate for fluids of any Prandtl number, Wärme- und Stoffübertragung 22 (1988) 159–168.